










## Article

# A Practical Superconducting DC Dynamo for Charging Conduction-Cooled HTS Magnet

Yujia Zhai <sup>1,2,3</sup> , Chunran Mu <sup>1,2,\*</sup> , Jinduo Wang <sup>1,2</sup> , Litong Zhu <sup>1,2</sup> , Tingkun Weng <sup>1,2</sup> , Zhuo Li <sup>1,2</sup> ,  
Xingzheng Wu <sup>1,2</sup> , Liufei Shen <sup>1,2</sup> , Jianhua Liu <sup>3</sup>  and Qiuliang Wang <sup>3</sup>

- <sup>1</sup> College of Electrical and Information Engineering, Hunan University, Changsha 410082, China; yz378@hnu.edu.cn (Y.Z.); wjd0120@hnu.edu.cn (J.W.); zlt0010@hnu.edu.cn (L.Z.); vontink@hnu.edu.cn (T.W.); lizhuo@hnu.edu.cn (Z.L.); xingzhengwu@hnu.edu.cn (X.W.); xiaofei482@hnu.edu.cn (L.S.)
- <sup>2</sup> Engineering Research Center of Power Transmission and Transformation Technology, Ministry of Education, Changsha 410082, China
- <sup>3</sup> Institute of Electrical Engineering, Chinese Academy of Sciences, Beijing 100190, China; liujianhua@mail.iee.ac.cn (J.L.); qiuliang@mail.iee.ac.cn (Q.W.)
- \* Correspondence: mcr@hnu.edu.cn

**Abstract:** At present, HTS magnets cannot operate in the real closed-loop persistent current mode due to the existence of joint resistance, flux creep, and AC loss of the HTS tape. Instead of using a current source, HTS flux pumps are capable of injecting flux into closed HTS magnets without electrical contact. This paper presents a practical superconducting DC dynamo for charging a conduction-cooled HTS magnet system based on a flux-pumping technique. To minimize heat losses, the rotor is driven by a servo motor mounted outside the vacuum dewar by utilizing magnetic fluid dynamic sealing. Different parameters, such as air gap and rotating speed, have been tested to investigate the best pumping effect, and finally, it successfully powers a 27.3 mH HTS non-insulated double-pancake coil to the current of 54.2 A within 76 min. As a low-cost and compact substitute for the traditional current source, the realization of a contactless DC power supply can significantly improve the flexibility and mobility of the HTS magnet system and could be of great significance for the technological innovation of future HTS magnets used in offshore wind turbines, biomedical, aerospace, etc.

**Keywords:** HTS magnets; conduction cooled; contactless magnetizing technology; DC dynamo



**Citation:** Zhai, Y.; Mu, C.; Wang, J.; Zhu, L.; Weng, T.; Li, Z.; Wu, X.; Shen, L.; Liu, J.; Wang, Q. A Practical Superconducting DC Dynamo for Charging Conduction-Cooled HTS Magnet. *Energies* **2024**, *17*, 2684. <https://doi.org/10.3390/en17112684>

Academic Editor: Armando Pires

Received: 15 April 2024

Revised: 24 May 2024

Accepted: 26 May 2024

Published: 31 May 2024



**Copyright:** © 2024 by the authors. Licensee MDPI, Basel, Switzerland. This article is an open access article distributed under the terms and conditions of the Creative Commons Attribution (CC BY) license (<https://creativecommons.org/licenses/by/4.0/>).

## 1. Introduction

Thanks to its higher current-transmission capacity and better mechanical properties under a high field, 2G high- $T_c$  superconducting (HTS) coated conductors (CC) represented by ReBCO tape are capable of providing technical support for the realization of steady-state high magnetic fields over 20 T and are extremely important for the technological innovation of HTS magnets in engineering application fields, such as aerospace, offshore wind turbines, biomedical, transportation, high-energy physics, etc. [1–4].

However, due to the presence of joint resistance, flux creep, and the AC loss of HTS tapes, current decays in the closed superconducting circuit, when it is in the superconducting state. For HTS magnets working in the closed-loop persistent current mode (PCM), current compensation is required. Normally, HTS magnets can be magnetized in two ways: through power supply and current leads, or through contactless flux pumps.

The conventional power supply is bulky and needs access to the current lead, which is connected between a room temperature and a low-temperature environment of the magnet, forming a huge leakage heat source. A leakage heat source is extremely detrimental to low-temperature maintenance of the superconducting magnets, particularly for high-current superconducting magnets, which greatly limits the application and development of future HTS magnets [5–7].

A superconducting flux pump is a contactless DC power-supply device for superconducting magnets that compensates for current decay and ensures magnetic field stability by pumping flux into the closed-loop circuit of superconducting magnets [2]. Many types of HTS flux pump devices have been proposed in recent decades, including the heat actuated flux pump [8–11], the rotating magnets flux pump [12–19], the linear type flux pump [20–23], and the transformer rectifier flux pump [24–27], all of which can effectively achieve DC magnetization for HTS coils or bulks.

However, the majority of those DC power-supply devices work under liquid-nitrogen cooling, which does not meet the needs of practical applications for conduction-cooled HTS magnets. In addition, although plenty of experiments have been presented to validate the technical feasibility of HTS flux pumps and the induced DC voltage [28–30], the microscopical level of the physical mechanism for the pumping effect still needs to be studied and understood in depth in order to obtain an optimum pumping field and make it practical for future large-scale applications of HTS magnets.

Therefore, for better-applying flux-pumping technology to the actual conduction-cooled closed-loop magnet, the heat loss of the flux-pump device should be minimized first. In the previous research, we found that a DC dynamo (rotating magnets flux pump) is well suited to be utilized in the conduction-cooled HTS magnets if we move its heating components outside the dewar by magnetic fluid dynamic sealing technology, and it will convert mechanical energy into electromagnetic energy. Thus, in the future, we can construct HTS magnets cooled by a Stirling cryocooler instead of the current GM cryocooler, making the whole magnet system compact and portable. By applying this new technique, the HTS magnet can be magnetized by a new segmented magnetization method, and its configuration can be optimized by using multiple DC dynamos.

We created the first-generation DC dynamo for a conduction-cooled HTS magnet in 2021 [1,12]. In order to obtain a better pumping effect, a more compact conduction-cooled HTS magnet system excited by the second generation (2G) DC dynamo was designed, fabricated, and tested at Hunan University in 2022, as shown in Figure 1a. The size of the dewar is reduced to lower the cooling burden of the cryocooler. Finally, we successfully pumped 54.2 A to the 27.3 mH conduction-cooled HTS magnet system within 76 min.

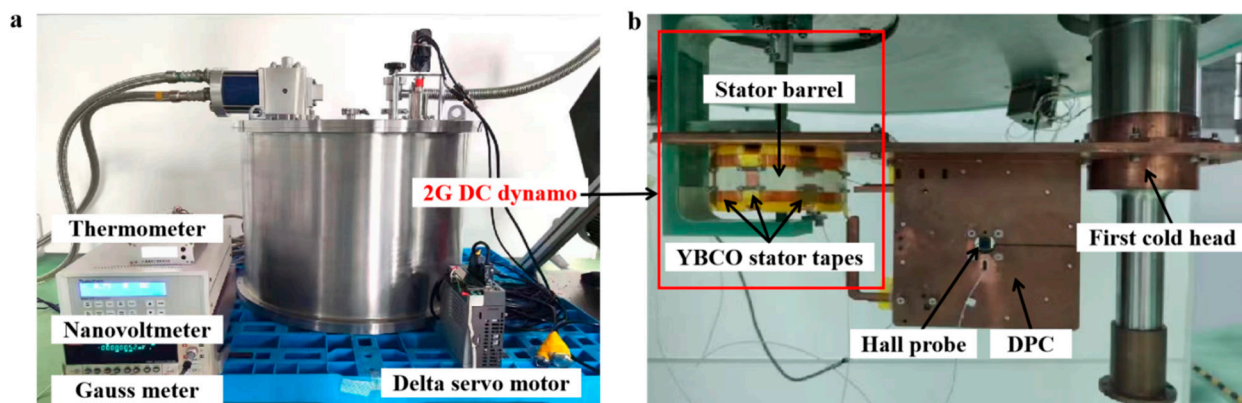


**Figure 1.** (a) Conduction-cooled HTS magnet system excited by the second-generation DC dynamo at Hunan University. (b) Structure of the 2G DC dynamo in the conduction-cooled HTS magnet system.

## 2. Experimental Setup

### 2.1. Structure of HTS Magnet System

The experimental setup of the magnet system consists of a compressor, a water-cooling unit, an ionization vacuum gauge, a 2G DC dynamo (Hunan University, Changsha, China), a double-pancake coil (SuperPower Inc., Glenville, NY, USA), a Delta servo motor (Delta, Shanghai, China), a KDE 412 GM cryocooler (CSSC Pride Cryogenic Technology Co., Ltd., Nanjing, China), and the measurement unit in Figure 1a,b. The Delta servo motor provides mechanical energy for the 2G DC dynamo, and a shaft is connected between the motor and

several disks with permanent magnets to turn mechanical energy into magnetic energy. The measurement unit is composed of a LakeShore 425 Gauss meter (Lake Shore Cryotronics, Inc., Westerville, OH, USA), a Keithley 2182 A Nanovoltmeter (Keithley, Cleveland, OH, USA), and a thermometer. The thermometer monitors the temperatures of four sensors that are installed inside the dewar. The Gauss meter tracks the magnetization of the DC dynamo, and the voltage at both ends of the YBCO tape is displayed on the Nanovoltmeter. LabVIEW is used to record the real-time amplitude of the magnetic field every 5 s.

## 2.2. Structure of 2G DC Dynamo

In the 2G experimental setup, the number of induction tapes is increased from one to eight in order to enhance the induced magnetic field (Figure 1b). The induction-tape barrel is designed and fabricated to accommodate eight stator tapes for parallel connection. The rotor is made up of two disks with a slot depth of 6 mm. Sixteen NdFeB permanent magnets with a 10 mm diameter and a 5 mm height are evenly distributed around the circumference of the disk. The diameters of the disks are designed from 72 to 74 mm to control the air gap ( $d$ ) between the surface of the permanent magnets and the induction tapes, which varies between 1 and 2 mm. The leakage rate is better than  $1.0 \times 10^{-10} \text{ Pa} \times \text{m}^3/\text{s}$ , and the vacuum degree is better than  $10^{-4} \text{ Pa}$ .

In this experiment, induction tapes are 10 mm wide CC coils from Shanghai superconducting technology Co., Ltd, Shanghai, China. Eight induction tapes are connected in parallel and fixed to the induction-tape barrel (Figure 1b). The load coil is a no-insulation (NI) double-pancake coil (DPC), wound by a 4 mm wide YBCO-coated conductor from SuperPower Inc. The critical current is 46.5 A at 77 K and 117–340 A at 40 K under a self-field.

## 2.3. Final Temperature Test

The main cooling device and elements are marked in Figure 2a. Four temperature sensors were installed inside the Dewar to monitor the temperature in real time and ensure that the system remains within the designed temperature range. By analyzing temperature readings from the thermometer, the cooling path of the flux pump can be inferred and determined to ensure the system is working properly.

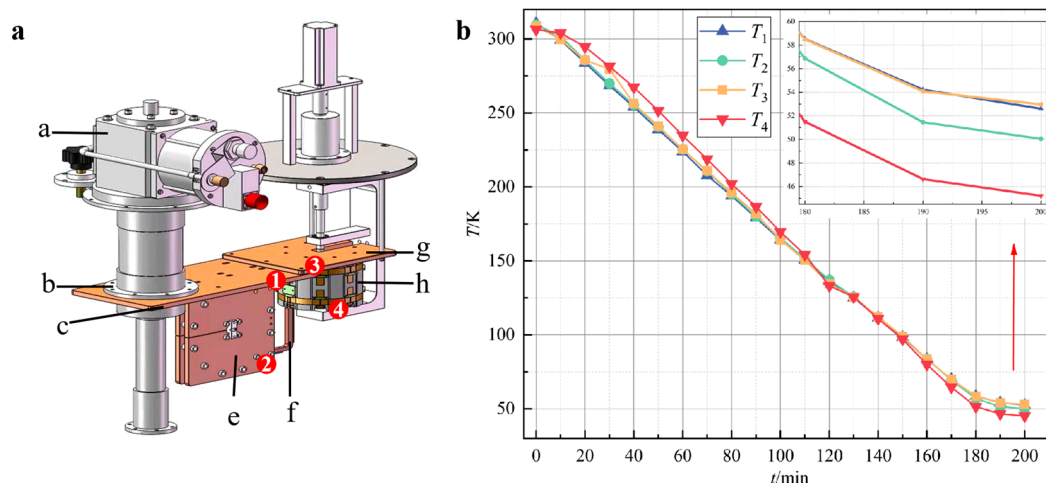


**Figure 2.** (a) The design of conduction-cooled path a–h and positions of thermometer 1–4. (a: GM cryocooler, b: first-stage cold head, c: rectangular copper cooling conductor, e: oxygen-free copper plates, f: L-shaped machined part, g: square copper cooling conductor, h: induction-tape barrel). (b) Schematic diagram of temperature changes of the magnet system.

The water-cooling equipment and compressor operated for approximately 200 min during the real cooling period of the system. The temperatures of the copper conductor c, the load DPC e, the copper conductor g, and the induction-tape barrel h are represented by  $T_1$ ,  $T_2$ ,  $T_3$ , and  $T_4$ , respectively, in Figure 2a. Through multiple tests, it was found that

the temperatures ultimately stabilized between 45 and 53 K in Figure 2b, which meets the magnetization margin of DPC  $I_{c40K} = 117\text{--}340$  A and protects tapes from quenching.

### 3. Experimental Results

Based on the 2G experimental setup, magnetization and demagnetization tests were conducted on a conduction-cooled HTS magnet system with varying air gaps and rotating speed, and the results are presented below.

#### 3.1. Different Air Gaps: 1 mm or 2 mm?

By adjusting the diameter of the disk, the air gap ( $d$ ) between the permanent magnets and the induction tapes can be adjusted to 1 mm or 2 mm. The saturation magnetic fields at 350 rpm were tested and recorded when  $d = 1$  and 2 mm in Figure 3a. It is found that after 209 min, the magnetic field reaches 2041 Gs at 350 rpm when  $d = 2$  mm. To increase the saturation field, the experiment was conducted by using large disks. When  $d = 1$  mm, the saturation magnetic fields at 350 rpm are recorded as 5586 Gs after 76 min. In addition, Figure 3b demonstrates that the saturation magnetic field at 500 rpm when  $d = 1$  mm is higher than that when  $d = 2$  mm. Therefore, it is obvious that a smaller air gap is better for an optimal pumping field.

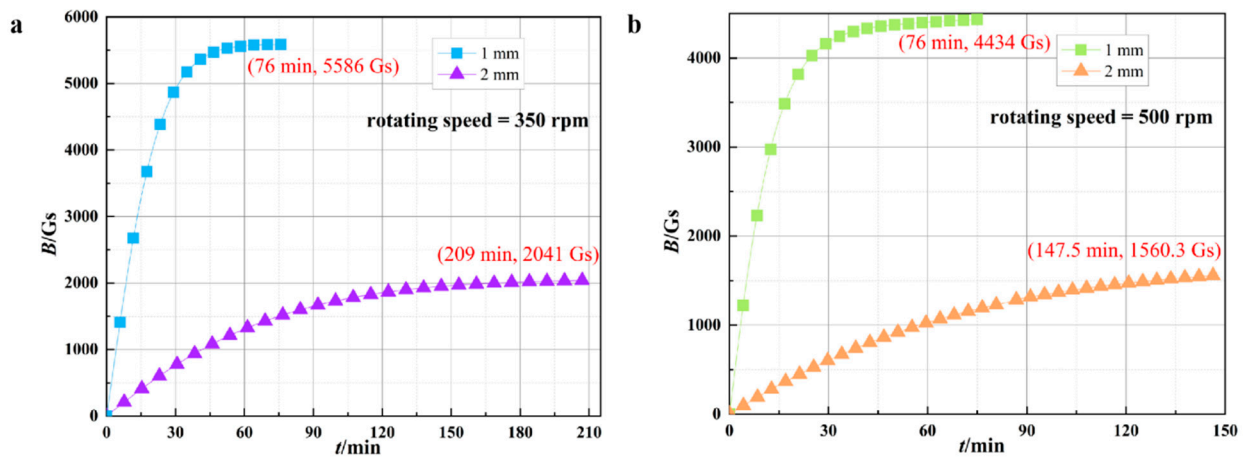


**Figure 3.** (a) Saturation magnetic field at 350 rpm when  $d = 1$  mm and  $d = 2$  mm. (b) Saturation magnetic field at 500 rpm when  $d = 1$  mm and  $d = 2$  mm.

Table 1 summarizes the magnetization and saturation results from the above experiments. The saturated magnetic field of 1 mm is more than twice that of 2 mm. It is found that the load coil can be excited by the 2G DC dynamo, and reducing the gap between the induction tapes and the magnets is an effective method to enhance the pumping effect. Based on the available experimental data, the maximum saturation magnetic field strength is 5586 Gs, which corresponds to 46.3% of the critical current at 45–53 K. The best magnetization is achieved when  $d = 1$  mm.

**Table 1.** Magnetization and saturation results at different gaps.

Air Gap (mm)	Rotating Speed (rpm)	Saturated Magnetic Field (Gs)	Induced Current (A)	Critical Current (%)
2	350	2041	19.8	16.9
1	350	5586	54.2	46.3
2	500	1560.3	15.1	12.9
1	500	4434	43.0	36.8



### 3.2. Different Rotating Speeds at 1 mm and 2 mm Air Gap

As can be seen in Section 3.1, it is found that it is not the greater the rotating speed of the dynamo, the better the magnetization effect could be. It can be considered that there should exist an optimal value of the rotating speed. At the optimal rotating speed, the magnetization rate is the fastest and the saturation magnetic field is the largest.

Figure 4a illustrates the magnetization process when  $d = 1$  mm over a period of 25 min at different rotating speeds from 200 rpm to 900 rpm. As can be seen, the magnetization rate reaches its peak at 350 rpm, with a maximum value of 26 Gs/min. When the rotating speed exceeds 350 rpm, the magnetization at 25 min ( $B_{25\text{min}}$ ) gradually decreases, despite the speed still increasing.

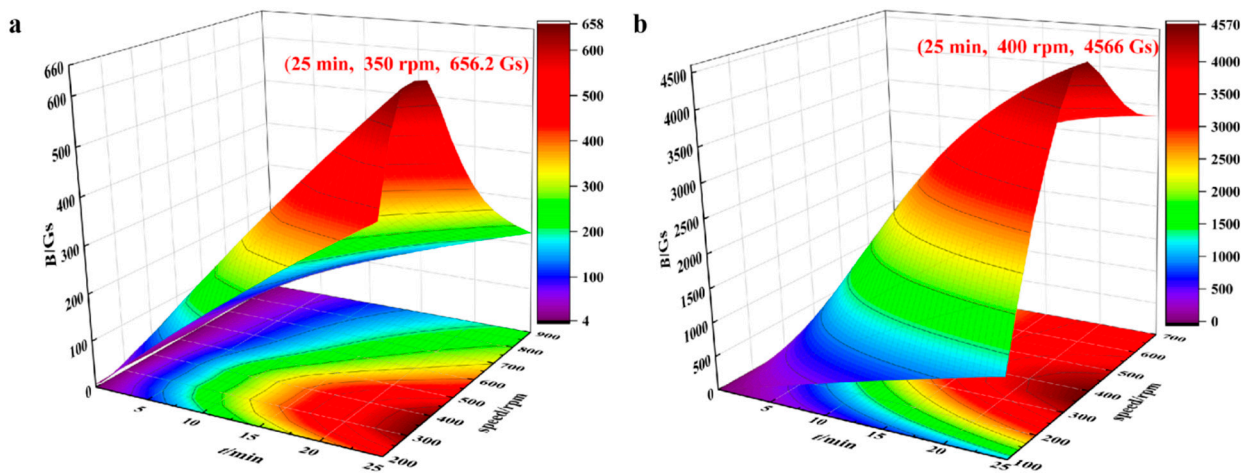


**Figure 4.** (a) Magnetization of small-disk experiment ( $d = 2$  mm) at different rotating speeds. (b) Magnetization effect of large turntable experiment at different rotating speeds ( $d = 1$  mm).

The magnetization process at different rotating speeds was displayed for 25 min when  $d = 1$  mm in Figure 4b. The magnetization rate is found to peak at 182.64 Gs/min at a rotating speed of 400 rpm, and the magnetization rates of the other rotating speeds are all less than that of 400 rpm. Based on Figure 4a,b, it can be observed once more that the magnetization effect is better when  $d = 1$  mm, and thus, the subsequent experiments are carried out with the fixed air gap.

In Figure 5a, the curve slope is maximum and almost constant during the first 5 min. Therefore, the fastest magnetization rate is the increased magnetic field during this time divided by the time 5 min. The fastest magnetization rate increases with the increasing rotating speed, as shown in Figure 5c. The average magnetization rates for various rotating speeds were determined by testing all the magnetization up to saturation at the optimal air gap. The saturation field and the average magnetization rate at different rotating speeds when  $d = 1$  mm can be shown in Figure 5b,d, which are both maximum at 350 rpm and smaller, as the rotating speeds spread to both sides.

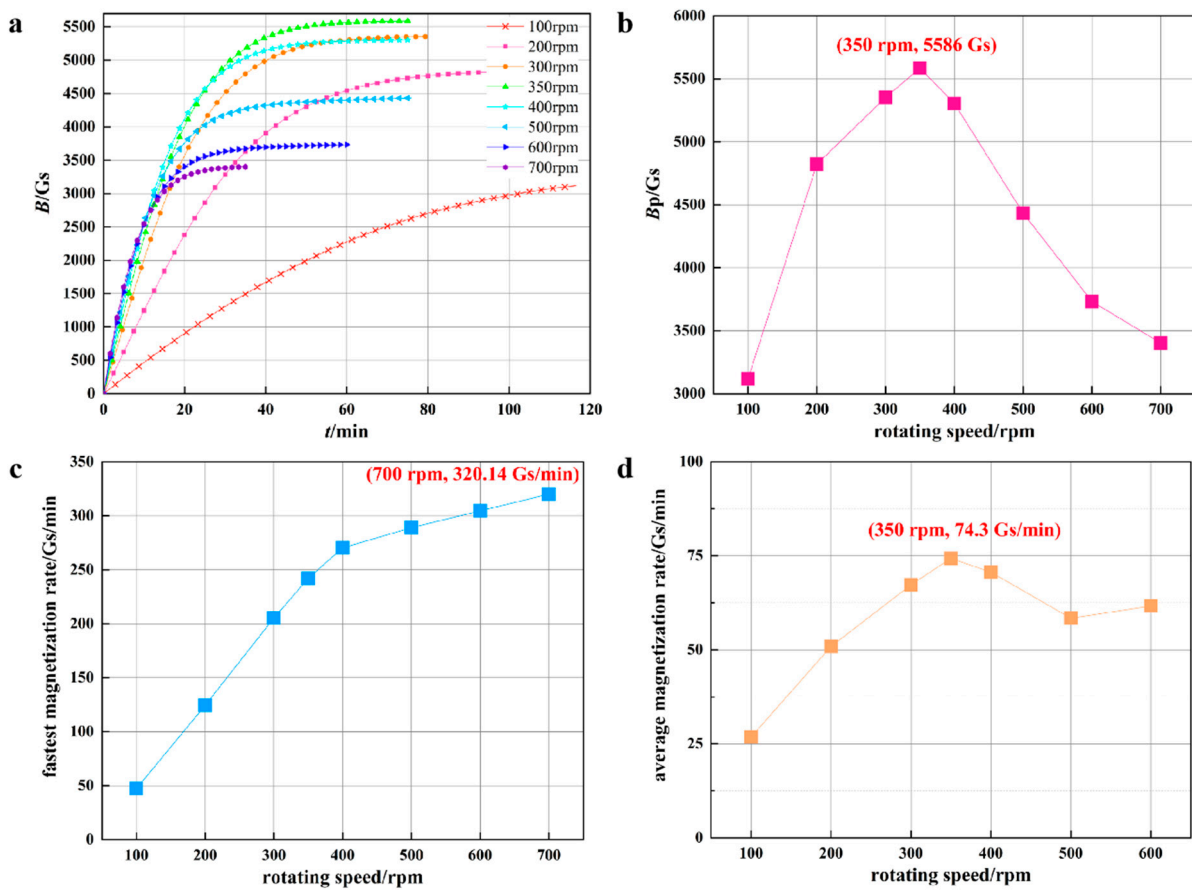


**Figure 5.** (a) Magnetization diagram with different rotating speeds when  $d = 1$  mm. (b) Saturation magnetic field at different rotating speeds. (c) Fastest magnetization rate at different rotating speeds. (d) Average magnetization rate at different rotating speeds.

### 3.3. Demagnetization Rate

A demagnetization experiment, when  $d = 1$  mm, was performed by reverse turning of the server motor, and a demagnetization diagram and the average demagnetization rate with different reverse rotating speeds are shown in Figure 6a,b. The curve slope at different rotating speeds reveals that the slowest demagnetization occurs at 100 rpm. The average demagnetization rate increases as the speed increases from 100 to 700 rpm, and the value at 700 rpm is about eight times greater than that at 100 rpm.

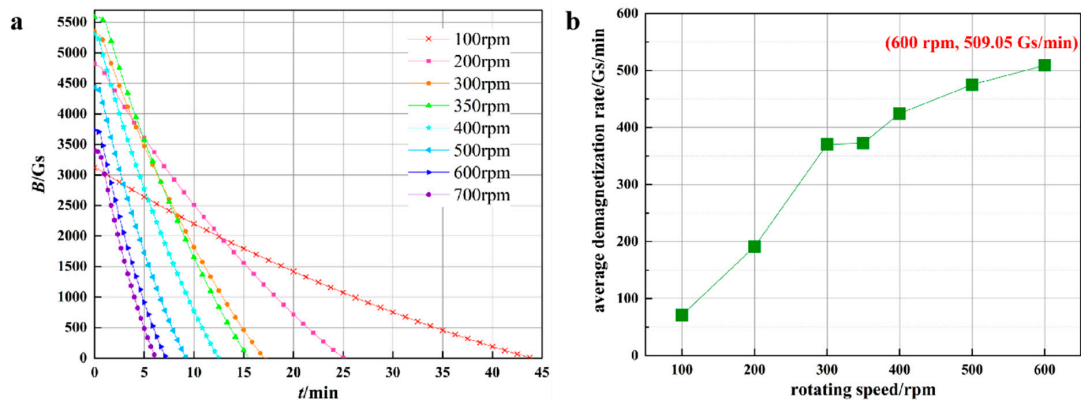


**Figure 6.** (a) Demagnetization diagram with different rotating speeds when  $d = 1$  mm. (b) Average demagnetization rate at different rotating speeds.

#### 4. Theory of HTS Flux Pump

The closed-loop operation of conduction-cooled HTS magnets based on the flux-pumping effect is feasible by experimental verification. However, this pumping effect cannot be fully explained by the traditional electromagnetic induction theory [31,32]. Giaver was the first to propose the superconducting rectification effect, which could convert an AC electromagnetic field into a DC electromagnetic field, just like a DC transformer [33]. Recently, 2D/3D numerical calculations and experiments were presented to explain DC voltage  $V_{oc}$  and internal resistance  $R_{int}$  in the flux-pump effect [29,30,34,35]. To improve and complement the superconducting rectification mechanism from a microscopic perspective, this paper puts forward a novel macroscopic magnetic flux quantum diffusion-rectification theory, which provides a comprehensive explanation for the quantum phenomenon of AC magnetic field-induced DC voltage inside the superconducting tape.

When the applied magnetic field strength ( $H$ ) exceeds the lower critical magnetic field ( $H_{c1}$ ) of the type II superconductor, the superconducting tape enters a mixed state where the superconducting state and the normal state coexist. The normal core and the overall structure of the vortex current around it are usually referred to as the vortex structure. In a uniformly distributed magnetic field, the vortex structure is uniformly distributed in the superconductor, resulting in no net current generation, as in Figure 7a.

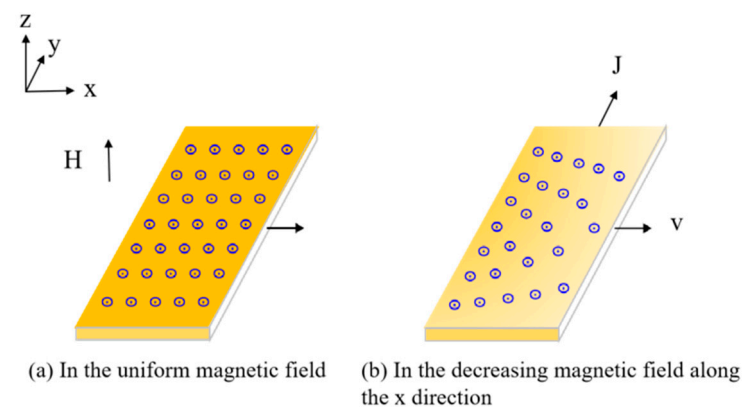


**Figure 7.** Magnetic flux quantum distribution and body current generation mechanism diagram.

Once the vortex structure or the applied magnetic field is not uniformly distributed, a macroscopic bulk current density  $J$  will be generated. The magnetic field  $H$  and the vortex density decrease along the  $x$ -direction in Figure 7b. At the interface where the two layers of vortex lines intersect, the current cannot cancel each other, which will generate a body current  $J$  in the  $y$ -direction [36]. The non-uniform flux quanta in a non-uniform magnetic field will form a vortex density gradient, resulting in a local diffusion effect. The vortex moves from the high magnetic field region to the low magnetic field region. After reaching the low magnetic field region, the vortex current decays, and the flux quanta annihilate. This process eventually leads to the generation of a macroscopic-induced DC current.

The electric field generated by the moving flux vortex is described as follows [36]:

$$E = v_L \times B = v_L \times n\phi_0 \quad (1)$$

where  $v_L$  is the velocity of the vortex,  $\phi_0$  is the quantum flux, and  $n$  is the flux number per unit area. According to formulation (1), the vortex will accelerate over time, and the electric field will increase accordingly. However, in the ideal type II superconductor, the electric field is constant, indicating that there exists a viscous resistance  $f_L$  in the process of flux motion [36].

$$f_L = \eta v_L = j\phi_0 = \frac{E}{\rho} \phi_0 \quad (2)$$

where  $\eta$  is the coefficient of viscosity,  $j$  is the transmission current density, and  $\rho$  is the magnetic flux flow resistance. The loss generated  $P = J \cdot E$ .

In order to prevent the motion of the flux vortex, when the Lorentz force of the flux vortex exceeds the pinning force in a non-ideal type II superconductor, the flux begins to move. Due to the magnetic field gradient and the body transmission current, there is no loss.

In general, the bulk current transmitted within the superconductor is generated exclusively by the asymmetry of the magnetic field and the gradient of the vortex density [37]. When HTS tape carries a DC current and is subjected to an AC magnetic field perpendicular to the direction of the current, dynamic resistance is generated, which is given by [38]:

$$R_d = \frac{2alf}{I_c} (B_a - B_{a,th}) \quad (3)$$

$$B_{a,th} = \frac{2.4642\mu_0 J_c t}{\pi} (1 - I_t/I_c) \quad (4)$$

where  $a$ ,  $l$ , and  $t$  represent the width, length, and thickness of the superconductor, respectively;  $f$  and  $B_a$  represent the frequency and magnitude of the applied AC field;  $B_{a,th}$  is the threshold field below which dynamic resistance cannot be generated; and  $I_c$  and  $J_c$  are the critical current and critical current density of the superconductor, respectively. Inside the superconductor, there is an induced DC voltage whose magnitude is positively correlated with the gradient of the traveling magnetic field. To increase the magnetization saturation current of the DPC, the driving voltage  $V_{oc}$  should be increased, and the dynamic resistance  $R_d$  should be reduced.

In this experiment, the diameter of the rotating disk determines the air gap  $d$  and, hence, the applied traveling magnetic field gradient. The induced DC current increases with the decreasing  $d$ .

## 5. Analysis for Large Inductance Applications

In practice, the value of inductance for HTS magnets is relatively large. For example, a 15,000 Gs HTS magnet with a bore diameter of 60 mm has an inductance of 1 H. The contactless magnetic flux rectification effect of the flux pump has only been tested and verified on a magnet with a smaller inductance value (27.3 mH). Therefore, this paper demonstrates whether a flux pump can be applied to HTS magnets with large inductance from both simulation analysis and theoretical derivation.

### 5.1. Simulation Analysis

The equivalent circuit of a 2G DC dynamo with load is shown in Figure 8a. The stator part of the DC dynamo can be represented by an open-circuit voltage  $V_{oc}$ , a dynamic resistance  $R_d$ , and a joint resistance  $R_c$ .  $L$  is the equivalent inductance of the superconducting magnets connected in series [13].

Based on the experimental data, the 2G DC dynamo can inject a maximum current  $I_{max}$  of 117 A at 40 K, with a joint resistance  $R_c$  of  $3 \times 10^{-6} \Omega$  and a variable resistance  $R_d$  of  $10^{-6} \Omega$ .

The current flowing in the loop is:

$$I(t) = (I_1 - I_{max})e^{\frac{(R_d+R_c)t}{L}} + I_{max} \quad (5)$$

where  $I_1$  is the initial value of the current in the circuit and is set to zero. The voltage across the coil load is:

$$V_{oc} - I(R_d + R_c) = L \frac{dI}{dt} \quad (6)$$

The inductance is:

$$L = \sum_{i=1}^n L_i \quad (7)$$

where  $L_i$  is the value of the  $i$ -th inductor. The  $I$ - $t$  image of the effect of small inductance (single load coil) and large inductance (50 load coils linked in series) on the circuit, according to the above formulations, is shown in Figure 8b.



The ramping time depends on the number of load coils or the inductance of the magnet. The fewer the load coils, the faster the ramping speed. When the number of load coils varies, the final magnetic field strengths are equivalent.

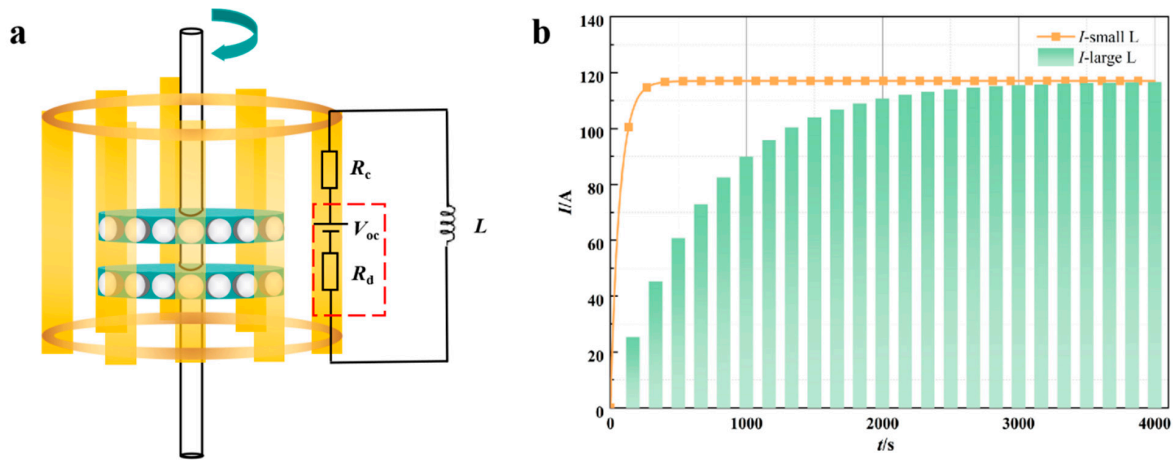


**Figure 8.** (a) Equivalent circuit diagram of the 2G DC dynamo. (b) Effect of small inductance and large inductance on the circuit.

### 5.2. Theoretical Derivation

To better apply the 2G flux pump in NI HTS magnets with large inductance, the black-box method is employed to investigate the pumping system. The flux pump is treated as a black box with load coils attached at both ends, and the power of the magnetization system is calculated by evaluating the load magnets. The magnetization rate of the load coil is measured, and ANSYS finite element simulation is used to introduce an induced magnetic field of 103 Gs for 1 A induced current.

$$B = 0.0103I \tag{8}$$

The power of a magnetic flux pump is:

$$P = \frac{W}{t} = \frac{\frac{1}{2}LI^2}{t} \tag{9}$$

Further, we can get:

$$P = \frac{L\left(\frac{B}{0.0103}\right)^2}{2t} = \frac{LB^2}{21218t} \times 10^8 \tag{10}$$

Hence, based on the black-box method, the power of the 2G flux-pump system is calculated to be 8.8 mW.

To determine whether the system can be used in magnets of a large inductance, the power of the 2G flux-pump HTS closed-loop operation system is kept constant. According to Equations (9) and (10), the following equation can be derived:

$$\frac{L_1 I_1^2}{t_1} = \frac{L_2 I_2^2}{t_2} \tag{11}$$

$$\frac{L_1 B_1^2}{t_1} = \frac{L_2 B_2^2}{t_2} \tag{12}$$

Set  $L_1 = 27.3$  mH,  $B_1 = 5586$  Gs,  $I_1 = 54.2$  A,  $t_1 = 76$  min = 4560 s, and  $L_2 = 0.65$  H. At the same magnetic field strength and induced current, the magnetization time for magnets

with a large inductance ( $L_2$ ) is longer than that with a small inductance ( $L_1$ ), which can be obtained as follows:  $t_2 = 30.16$  h.

Consequently, this DC dynamo can be applied to conduction-cooled HTS magnets with proper inductance under three working modes: magnetization mode, compensation mode, and demagnetization mode. In the magnetization mode, it can excite a 0.65 H magnet to 50,000 Gs in about 30 h. In the compensation mode, the load current can be compensated quickly and effectively. Moreover, the 2G flux pump can realize rapid demagnetization for the load coil by reverse rotation of the motor.

## 6. Conclusions

In this study, we demonstrated a conduction-cooled HTS magnet system excited by a 2G DC dynamo and operating at 45–53 K, with a current of up to 54.2 A and an inductance of 27.3 mH.

On the basis of the theoretical analysis and equation derivation, we verified that the 2G DC dynamo can be applied to magnets with large inductance. The novel DC dynamo is portable, compact, and capable of meeting the needs for the superconducting magnet magnetization and compensation requirements by converting mechanical energy into electrical energy without generating extra heat loss. Its realization implies the possibility of a new practical method of magnetizing HTS magnets, which can replace the traditional expensive bulky DC power supply and current leads for HTS magnets. The maturity of this contactless magnetization technology will encourage the endless development and application of HTS magnets in biomedical, aerospace, offshore wind turbines, high-energy physics, large science projects, fusion, and many other fields, resulting in significant redevelopment of steady-state strong magnetic field equipment.

However, it still has some imperfections that need to be improved in future work for commercial applications.

(1) The internal heat leakage of the flux pump is caused by the heat produced by the joint resistance between the induction tapes and the connections between the induction tapes and the load. At present, stator tapes are in the form of multiple parallel connections to reduce  $R_d$ . In the next stage, we will focus on improving the welding technique of the joint resistance to ensure that the resistance value reaches the level of  $n\Omega$  magnitude so that a Stirling cryocooler with lower cooling power can be used.

(2) At present, most of the previous studies tend to investigate at the device level, ignoring the understanding of the intrinsic orientation of the flux-pumping phenomenon. As superconductivity is a macroscopic condensed behavior based on quantum mechanics, the effective motion of fluxon vortices induced by the traveling magnetic wave should be further explored, in order to achieve efficient macroscopic regulation of the fluxons and finally realize the optimization of all types of flux-pump devices, so that the pumping efficiency and maximum output power could be both improved.

**Author Contributions:** Conceptualization, Y.Z., C.M. and Z.L.; methodology, J.L. and Q.W.; formal analysis and investigation, X.W., L.S. and T.W.; data curation, J.W. and L.Z.; writing—original draft preparation, C.M.; writing—review and editing, Y.Z.; funding acquisition, Y.Z. and C.M. All authors have read and agreed to the published version of the manuscript.

**Funding:** This research was funded in part by the National Natural Science Foundation of China under Grant 52177019, in part by the Young Elite Scientists Sponsorship Program by CAST under Grant 2021QNR001, in part by the Hunan Provincial Natural Science Foundation Outstanding Youth Program under Grant 2021JJ20013, and in part by the Hunan Province Innovation Platform Talent Program-Huxiang Young Talents under Grant 2021RC3058.

**Data Availability Statement:** Data are contained within the article.

**Acknowledgments:** This work was supported by the Superconductivity and New Energy R&D Centre of Hunan University, Institute of Electrical Engineering Chinese Academy of Sciences, Northwest Nuclear Technology Institute, and Engineering Research Center of Power Transmission and Transformation Technology, Ministry of Education of China.

**Conflicts of Interest:** The authors declare no conflicts of interest.

## References

1. Wang, Q.; Liu, J.; Zheng, J.; Qin, J.; Ma, Y.; Xu, Q.; Wang, D.; Chen, W.; Qu, T.; Zhang, X.; et al. Progress of ultra-high-field superconducting magnets in China. *Supercond. Sci. Technol.* **2022**, *15*, 023001. [[CrossRef](#)]
2. Coombs, T.; Geng, J.; Fu, L.; Matsuda, K. An Overview of Flux Pumps for HTS Coils. *IEEE Trans. Appl. Supercond.* **2016**, *26*, 4600806. [[CrossRef](#)]
3. Coombs, T.A. Superconducting flux pumps. *J. Appl. Phys.* **2019**, *125*, 230902. [[CrossRef](#)]
4. Zhai, Y.; Tan, Z.; Liu, X.; Shen, B.; Coombs, T.A.; Wang, F. Research progress of contactless magnetization technology: HTS flux pumps. *IEEE Trans. Appl. Supercond.* **2020**, *30*, 4602905. [[CrossRef](#)]
5. Hamilton, K.; Cole, R.M.; Geng, J.; Bumby, C.; Carnegie, D.; Badcock, R. Practical Estimation of HTS Dynamo Losses. *IEEE Trans. Appl. Supercond.* **2020**, *30*, 4703105. [[CrossRef](#)]
6. Soomro, W.A.; Guo, Y.; Lu, H.; Jin, J.; Shen, B.; Zhu, J. Experimental Setup for Measurement of AC Loss in HTS under Rotating Magnetic Field. *Energies* **2022**, *15*, 7454. [[CrossRef](#)]
7. Zhou, P.; Dos, S.G.; Ghabeli, A.; Grilli, F.; Ma, G. Coupling electromagnetic numerical models of HTS coils to electrical circuits: Multi-scale and homogeneous methodologies using the—Formulation. *Supercond. Sci. Technol.* **2022**, *35*, 115005. [[CrossRef](#)]
8. Yan, Y.; Hong, Z.; Li, Q.; Xian, W.; Yuan, W.; Coombs, T.A. Thermally Actuated Magnetization Method in High Temperature Superconductor Bulks. *IEEE Trans. Appl. Supercond.* **2010**, *20*, 1823–1826. [[CrossRef](#)]
9. Zhai, Y.; Matsuda, K.; Coombs, T.A. Modeling and simulation of thermomagnetic materials for thermally actuated magnetization flux pumping method. *IEEE Trans. Appl. Supercond.* **2016**, *26*, 0605505. [[CrossRef](#)]
10. Zhai, Y.; Huang, Z.; Zhong, Z.; Coombs, T.A. Measurement and Analysis of Thermal Materials in the Thermally Actuated Magnetization Flux Pumping Method. *IEEE Trans. Appl. Supercond.* **2015**, *25*, 8801105. [[CrossRef](#)]
11. Zhai, Y.; Hsu, C.H.; Spaven, F.; Zhang, M.; Wang, W.; Coombs, T.A. Soft Ferrite Used as Thermal-Magnetic Conversion Intermedium in the Flux Pumping Technology. *IEEE Trans. Appl. Supercond.* **2013**, *23*, 7800104. [[CrossRef](#)]
12. Zhai, Y.; Niu, C.; Liu, X.; Wang, F.; Liu, J.; Wang, Q. Conduction-Cooled HTS Magnets Closed-Loop System Excited by a Rotating Magnets Flux Pump. *IEEE Trans. Appl. Supercond.* **2022**, *32*, 4601605. [[CrossRef](#)]
13. Zhenan, J.; Chris, W.B.; Rodney, A.B.; Sung, H.-J.; Long, N.J.; Amemiya, N. Impact of flux gap upon dynamic resistance of a rotating HTS flux pump. *Supercond. Sci. Technol.* **2015**, *28*, 115008. [[CrossRef](#)]
14. Ma, J.; Geng, J.; Gawith, J.; Zhang, H.; Li, C.; Shen, B.; Dong, Q.; Yang, J.; Chen, J.; Li, Z.; et al. Rotating Permanent Magnets Based Flux Pump for HTS No-Insulation Coil. *IEEE Trans. Appl. Supercond.* **2019**, *29*, 1–6. [[CrossRef](#)]
15. Hoffmann, C.; Pooke, D.; Caplin, A.D. Flux pump for HTS magnets. *IEEE Trans. Appl. Supercond.* **2011**, *21*, 1628–1631. [[CrossRef](#)]
16. Jiang, Z.; Hamilton, K.; Amemiya, N.; Badcock, R.A.; Bumby, C.W. Dynamic resistance of a high-Tc superconducting flux pump. *Appl. Phys. Lett.* **2014**, *105*, 112601. [[CrossRef](#)]
17. Lee, S.; Kim, W.-S.; Kim, Y.; Lee, J.-Y.; Park, S.-H.; Hong, G.-W.; Kim, S.; Han, J.; Hwang, Y.J.; Choi, K. Persistent current mode operation of a 2G HTS coil with a flux pump. *IEEE Trans. Appl. Supercond.* **2016**, *26*, 1–4. [[CrossRef](#)]
18. Chris, W.B.; Rodney, A.B.; Hae-Jin, S.; Kim, K.-M.; Jiang, Z.; Pantoja, A.E.; Bernardo, P.; Park, M.; Buckley, R.G. Development of a brushless HTS exciter for a 10 kW HTS synchronous generator. *Supercond. Sci. Technol.* **2016**, *29*, 024008. [[CrossRef](#)]
19. Hamilton, K.; Pantoja, A.E.; Storey, J.G.; Jiang, Z.; Badcock, R.A.; Bumby, C.W. Design and performance of a “Squirrel-Cage” dynamo-type HTS flux pump. *IEEE Trans. Appl. Supercond.* **2015**, *28*, 5205705. [[CrossRef](#)]
20. Fu, L.; Matsuda, K.; Baghdadi, M.; Coombs, T. Linear Flux Pump Device Applied to High Temperature Superconducting (HTS) Magnets. *IEEE Trans. Appl. Supercond.* **2015**, *25*, 4603804. [[CrossRef](#)]
21. Lin, F.; Koichi, M.; Tim, C. Linear Flux Pump Device Applied to HTS Magnets: Further Characteristics on Wave Profile, Number of Poles, and Control of Saturated Current. *IEEE Trans. Appl. Supercond.* **2016**, *26*, 0500304. [[CrossRef](#)]
22. Bai, Z.; Yan, G.; Wu, C.; Ding, S.; Chen, C. A novel high temperature superconducting magnetic flux pump for MRI magnets. *Cryogenics* **2010**, *50*, 688–692. [[CrossRef](#)]
23. Fu, L.; Matsuda, K.; Lecrevisse, T.; Iwasa, Y.; Coombs, T. A flux pumping method applied to the magnetization of YBCO superconducting coils: Frequency, amplitude and waveform characteristics. *Supercond. Sci. Technol.* **2016**, *29*, 04LT01. [[CrossRef](#)] [[PubMed](#)]
24. Gawith, J.; Geng, J.; Ma, J.; Shen, B.; Li, C.; Coombs, T.A. HTS Transformer–Rectifier Flux Pump Optimization. *IEEE Trans. Appl. Supercond.* **2019**, *29*, 5501605. [[CrossRef](#)]
25. Zhou, P.; Ma, G.; Deng, Y.; Nie, X.; Zhai, Y.; Liu, K.; Zhang, H.; Li, Y. A Contactless Self-Regulating HTS Flux Pump. *IEEE Trans. Appl. Supercond.* **2020**, *30*, 3603006. [[CrossRef](#)]
26. Geng, J.; Coombs, T.A. Mechanism of a high-Tc superconducting flux pump: Using alternating magnetic field to trigger flux flow. *Appl. Phys. Lett.* **2015**, *107*, 142601. [[CrossRef](#)]
27. Geng, J.; Matsuda, K.; Fu, L.; Shen, B.; Zhang, X.; A Coombs, T. Operational research on a high-Tc rectifier-type superconducting flux pump. *Supercond. Sci. Technol.* **2016**, *29*, 035015. [[CrossRef](#)]
28. Bumby, C.W.; Jiang, Z.; Storey, J.G.; Pantoja, A.E.; Badcock, R.A. Anomalous open-circuit voltage from a high-Tc superconducting dynamo. *Appl. Phys. Lett.* **2016**, *108*, 122601. [[CrossRef](#)]

29. Mataira, R.; Ainslie, M.; Pantoja, A.E.; Badcock, R.; Bumby, C. Mechanism of the high-*t*c superconducting dynamo: Models and experiment. *Phys. Rev. Appl.* **2020**, *14*, 024012. [[CrossRef](#)]
30. Ghabeli, A.; Pardo, E.; Kapolka, M. 3D modeling of a superconducting dynamo-type flux pump. *Sci. Rep.* **2021**, *11*, 10296. [[CrossRef](#)]
31. Campbell, A. Dynamic Resistance and Flux Pumping. *Preprints* **2019**, 2019050253.
32. Geng, J.; Li, C.; Coombs, T.A. A fast AC field controlled impedance in HTS coated conductors: Response speed and electric field value. *IEEE Trans. Appl. Supercond.* **2017**, *27*, 5000305. [[CrossRef](#)]
33. Giaever, I. A dc transformer. *IEEE Spectr.* **1966**, *3*, 9. [[CrossRef](#)]
34. Leonid, P.; Vladimir, S. Two-Dimensional Model of a High-Tc Superconducting Dynamo. *IEEE Trans. Appl. Supercond.* **2021**, *31*, 5201107. [[CrossRef](#)]
35. Mataira, R.C.; Ainslie, M.D.; Badcock, R.A.; Bumby, C.W. Origin of the DC output voltage from a high-Tc superconducting dynamo. *Appl. Phys. Lett.* **2019**, *114*, 162601. [[CrossRef](#)]
36. Wang, Q. *High Magnetic Field Superconducting Magnet Science*; Bai, C.: Beijing, China, 2008; pp. 198–200.
37. Zhai, Y.; Mu, C.; Zhu, L.; Wang, J.; Li, Z.; Weng, T.; Liu, J.; Wang, Q. Research Progress of Conduction-Cooled HTS Magnets Wireless Charging Technology-HTS Flux Pumps. *IEEE Trans. Appl. Supercond.* **2024**, *34*, 5200104. [[CrossRef](#)]
38. Jiang, Z.; Toyomoto, R.; Amemiya, N.; Zhang, X.; Bumby, C.W. Dynamic resistance of a high-*t*c coated conductor wire in a perpendicular magnetic field at 77 k. *Supercond. Sci. Technol.* **2016**, *30*, 03LT01. [[CrossRef](#)]

**Disclaimer/Publisher's Note:** The statements, opinions and data contained in all publications are solely those of the individual author(s) and contributor(s) and not of MDPI and/or the editor(s). MDPI and/or the editor(s) disclaim responsibility for any injury to people or property resulting from any ideas, methods, instructions or products referred to in the content.